ACTA STEREOL 1998; 17/1: 99-105
ORIGINAL SCIENTIFIC PAPER

MORPHOLOGICAL STUDY METHOD OF THE SWELLING OF RADIATED UO_2 AFTER THERMAL TREATMENT

Michel COSTER*, Isabelle ZACHARIE#

*LERMAT, UPRESA CNRS 6004, ISMRA, 6 Bd Maréchal Juin, 14050 Caen Cedex, France
#CEA/SACLAY, DRN-DRE-SRO-SIEN, 91191 Gif sur Yvette Cedex, France

SUMMARY

Any incident can arise in a pressurised water nuclear reactor. It can provoke a temporary increase of the temperature. In these conditions, fission gases diffuse rapidly and form bubbles specially in grain boundaries. These bubbles participate in the swelling of the irradiated material. These increases of temperature have been simulated in laboratory by thermal treatment on irradiated materials. A morphological study is necessary to understand the phenomenon and to allow the construction of a model of swelling.
The goal of this paper is to propose a method based on automatic image analysis that allows to quantitatively characterise the microstructure of the polycrystalline uranium oxide after intergranular swelling.
Irradiated and annealed samples are polished and observed by scanning electron microscope. An automatic threshold method is used to obtain the binary bubble image. Grain boundaries are reconstructed from bubbles by using mathematical morphology operators (closing, distance function, watershed...). One can thus count bubbles per boundary length unit and know the specific boundaries perimeter of grains.
An observation of the intergranular fracture surface shows that the distribution of bubble size is narrow. Their shape is approximately constant. That allows to use a stereometric relationship and to estimate the number of bubbles by unit of grain boundary surface from polished sections.
These stereological parameters are introduced in the model of swelling which has been validated experimentally.

Key words : Nuclear fuel, swelling, ceramics, mathematical morphology, stereology.

INTRODUCTION

Under normal pressurised water nuclear reactor (PWR) operating conditions, the fission products arising in the uranium oxide remain trapped by insertion or substitution in the fuel matrix. Variation of volume or swelling caused by the formation of such solid and gaseous fission products is slight. In abnormal conditions, a power transient appears. It corresponds to an increase in the temperature at the centre of the fuel. Under the effect of temperature and thermal gradient, fission gases can diffuse and precipitate, creating gas bubbles in the fuel.

These bubbles cause substantial swelling of the pellets. A morphological study is necessary to understand this swelling and to allow the construction of a model.
The goal of this paper is to describe an automatic image analysis method to characterise quantitatively the microstructure of polycrystalline uranium oxide after swelling.

MATERIAL, METALLOGRAPHY AND ACQUISITION OF IMAGES

To simulate these abnormal conditions, samples of uranium oxide derived from PWR fuel after two normal operating cycles, were subjected to thermal treatment in a furnace at temperatures between 1130°C and 1715°C for times between 5 mn and 10 h, (Zacharie, 1997; Zacharie *et al*, 1998a, Zacharie *et al*,1998b).
Fractured samples, before and after thermal treatment, were impregnated with Araldite under vacuum. They were then pre-polished in water using successively 200, 400 and 600 grade abrasive papers for a few minutes, then with hyprocel felt with diamond compounds of particle sizes of 8 µm and then 2 µm, for 20 mn. Finally, flush felt was used with a 1 µm particle size solution for 1 mn.
Then, these metallographic samples were observed and analysed with a scanning electron microscope, (figure1). The scanning electron microscope examinations show the presence of intergranular bubbles in all the treated samples. At 1410°C for 5 mn and 1130°C for 300 mn, all the grain boundaries can be distinguished. Regarding metallographic observations for higher thermal treatments, the bubbles are in sufficient quantities to localise all the grain boundaries within 5 mn. Moreover, the intragranular bubbles, which are smaller in size, are only observable for a small number of very high temperature treatments.
Irradiated and thermally processed samples have been fractured (figure 2). The observation of fracture surfaces indicates that bubbles correspond to a distribution of relatively narrow size.
Then, images are digitalised directly from scanning electron microscope using image processing software, OPTIMAS©.

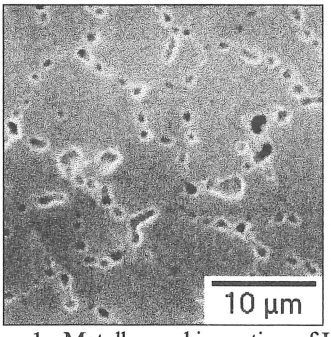

Figure 1 : Metallographic section of UO_2 sample observed by SEM.

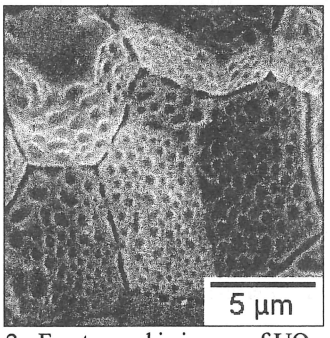

Figure 2 : Fractographic image of UO_2 sample observed by SEM.

IMAGE PROCESSING

The image processing is divided in two steps. During the first step performed with OPTIMAS, grey tone images are transformed in binary images by an automatic threshold. Among the methods based on the analysis of the histogram, the method of maximisation of the entropy gives the best results.

This method consists in maximising the entropy of the thresholded image, in order to render maximum contrasts between the classes, (Zeboudj, 1988; Coster and Chermant, 1989). The entropy function in a class C whose grey levels vary from p to q (p<q) is defined by :

$$H(C) = -\sum_{p}^{q} \frac{h(i)}{N} \ln\left(\frac{h(i)}{N}\right) \quad (1)$$

with : h(i), the number of pixels having the grey level i, and N the number of pixels in the class C. The entropy of the image is the sum of the entropies of each class. In the case of a unique threshold between two classes C_1 and C_2, the entropy of the image is given by :

$$H(k) = -\sum_{0}^{k} \frac{h(i)}{N(1)} \ln\left(\frac{h(i)}{N(1)}\right) - \sum_{k+1}^{max} \frac{h(i)}{N(2)} \ln\left(\frac{h(i)}{N(2)}\right) \quad (2)$$

The threshold t is the level corresponding to H(k) maximum.
Each binary image is then stocked under the form of a .BMP file to be processed by the MICROMORPH© software.
The second step consist of the construction of the grains boundaries from the not etched metallographic section. This processing is built from the following assumptions :

- the bubbles are only in inter-granular position,
- the ceramic grains are approximately convex.

In these conditions, grain boundaries will be obtained by applying the following processing, based on mathematical morphology, (Coster and Chermant, 1989; Serra, 1982) :

- the binary image is first filtered by hole filling, then by an opening of size 1, (figure 3 : image P'),
- the image P' is then inverted; so, one builds the image of distances of the image $(P')^C$.

This distance image is used to segment the image P' according to a watershed method, (Beucher and Meyer, 1992).

- on the inverted image (image D : figure 4), the h-minima are searched and are stored in the binary image Bm, (Grimaud, 1991); the h-minima are obtained by reconstructing the image (D + h) over the image D; one prefers to use the h-minima rather than the minima which are more sensitive to the noise; the image Bm is then dilated by an hexagon of size d so as to connect the very close h-minima, (figure 5); parameters h and d are determined experimentally to obtain an image of markers M correctly filtered,
- the watershed lines of the image D from marker M is then built, (image B2); after inversion, the image B2 is filtered by an hexagonal erosion of size e, followed by a skeleton by influence zone SKIZ); marker and watershed line are in white, the distance in grey and bubbles in black in figure 6,.
- the image Br is slightly over-segmented; that is due to two phenomena : i) some intragranular bubbles that the procedure considers as intergranular; this situation is possible only for temperatures higher than 1700°C; ii) the existence of slightly concave grains; despite the care brought to the development of the procedure of segmentation, a small semi-automatic correction is necessary,
- manually, one cuts superfluous grain boundaries that are completely eliminated by a clipping followed by a SKIZ and an inversion of the image; one obtains thus the corrected image of grain boundaries in the absence of bubble (image J'); by union with P', the image with grain boundaries and bubbles is then obtained, (figure 7).

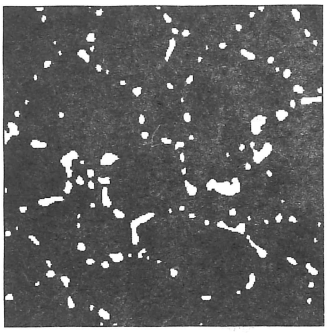

Figure 3 : Filtered image (P') obtain after automatic threshold of figure 1.

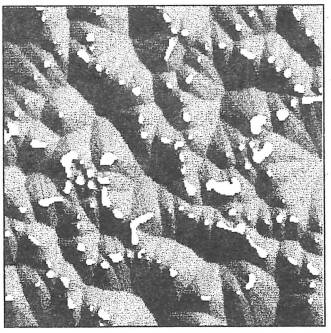

Figure 4 : Inverted distance image (D) of P'.

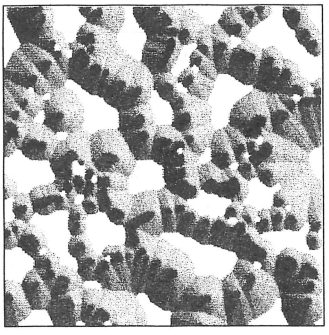

Figure 5 : Inverted distance image (D) and dilated h-minima.

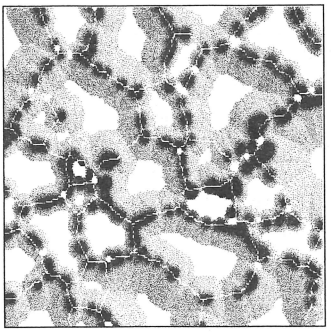

Figure 6 : Union of watershed lines ,corrected by erosion and SKIZ, with figure 5.

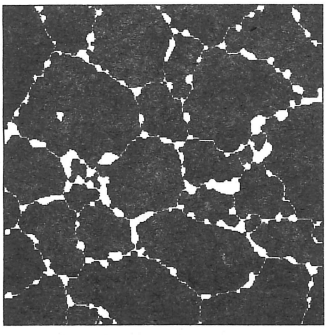

Figure 7 : Final result after some manual corrections followed by, a SKIZ and the union with P'.

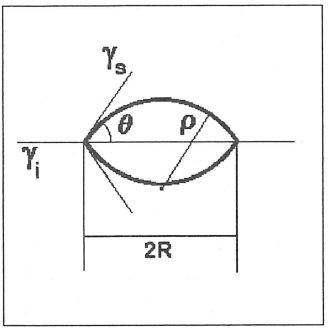

Figure 8 : Model of bubble with the different interfacial energies γ_i and γ_s. R is the radius of disk and ρ the radius of the spherical cap.

STEREOLOGICAL RELATIONSHIPS

Let P be the set of bubbles and J the set of grain boundaries in R^3. In the metallographic section Π, these sets become respectively $P' = P \cap \Pi$ and $J' = J \cap \Pi$. Table I gives the symbols and the definition of the parameters used in this stereological approach.

Table I : Symbol and definition of parameters.

$S_S(P \cap J)$	Area fraction of bubbles on grain boundaries J in R^3
$L_L(P' \cap J')$	Linear fraction of bubbles on grain boundaries J' in metallographic section
$L_A(J')$	Specific perimeter of grain boundaries J'
$L_A(P' \cap J')$	Specific perimeter of grain boundaries J' intersected by bubbles P'
$N_A(P' \cap J')$	Specific connectivity number of grain boundaries J' intersected by bubbles P'
$N_L(P' \cap J')$	Number of bubbles per unit length of grain boundaries J' in R^2
$N_S(P \cap J)$	Number of bubbles per unit area of grain boundaries J in R^3

The following relationships can be written without hypothesis on the analysed sets.

$$V_V(P) = A_A(P') \tag{3}$$

$$S_S(P \cap J) = L_L(P' \cap J') = \frac{L_A(P' \cap J')}{L_A(J')} \tag{4}$$

If one supposes that all bubbles have the same size and give a disk of radius R on the grain boundaries, one can calculate the area $\overline{S}(P)$ of the disk and the mean chord $\overline{L}(P')$ in the metallographic plane Π. Indeed, one has :

$$\overline{S}(P) = \pi R^2 \quad \text{and} \quad \overline{L}(P') = \frac{\pi}{2} R \tag{5}$$

Equations 5 lead to the equation 6 :

$$\overline{S}(P) = \frac{4}{\pi} (L(P'))^2 \tag{6}$$

One can also write :

$$S_S(P \cap J) = N_S(P \cap J) \cdot \overline{S}(P) \tag{7}$$

$$L_L(P' \cap J') = N_L(P' \cap J') \cdot \overline{L}(P') \tag{8}$$

According to the equation 4, equations 7 and 8 are equal. By replacing $\overline{S}(P)$ by its expression according to $\overline{L}(P')$, (equation 6), one can give a new expression of $N_S(P \cap J)$:

$$N_S(P \cap J) = \frac{\pi \cdot (N_L(P' \cap J'))^2}{4 \cdot L_L(P' \cap J')} \tag{9}$$

$N_L(P' \cap J')$ and $L_L(P' \cap J')$ can be transformed in more classical expressions 10 :

$$L_L(P' \cap J') = \frac{L_A(P' \cap J')}{L_A(J')} \quad \text{and} \quad N_L(P' \cap J') = \frac{N_A(P' \cap J')}{L_A(J')} \tag{10}$$

Then :

$$N_S(P \cap J) = \frac{\pi \cdot (N_A(P' \cap J'))^2}{4 \cdot L_A(J') \cdot L_A(P' \cap J')} \tag{11}$$

This last equation can be estimated from measurements on images J' and $(P' \cap J')$.
$N_V(P)$ can then be determine, as we have :

$$N_V(P) = S_V(J) \cdot N_S(P \cap J) = \frac{(N_A(P' \cap J'))^2}{L_A(P' \cap J')} \tag{12}$$

Because $V_V(P) = N_V(P) \cdot \overline{V}$, it is possible to calculate this expression from mean lenticular volume (figure 8), which is given by :

$$\overline{V} = \frac{2\pi}{3}(1-\cos\psi)^2 \cdot (2+\cos\psi) \cdot \rho^3 \quad \text{with} \quad \rho = \frac{R}{\sin\psi} \tag{13}$$

CONCLUSION : APPLICATION TO SWELLING

The swelling G can be defined from stereological parameters according to equation 14 :

$$G = \frac{V_V(P_f) - V_V(P_i)}{1 - V_V(P_i)} \tag{14}$$

where the index f represents the system after treatment and the index i, the system before treatment. The comparison between calculated value of volume fraction and the direct measurement are in good agreement since we have 15% of difference on the same sample. In these conditions, it is possible to use $N_S(P \cap J)$, estimated by equation 11, to follow the formation and the coalescence of bubbles during the thermal treatment. Figures 10 and 11 give the evolution of this parameter and swelling G as a function of time and temperature.

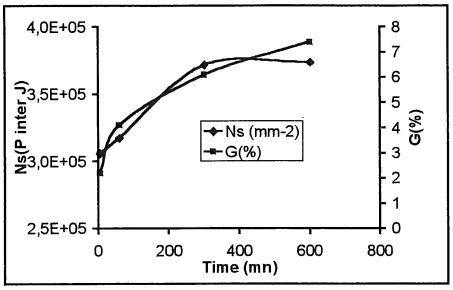

Figure 9 : Evolution of $N_S(P \cap J)$ and G as a function of time for a temperature of 1545°C.

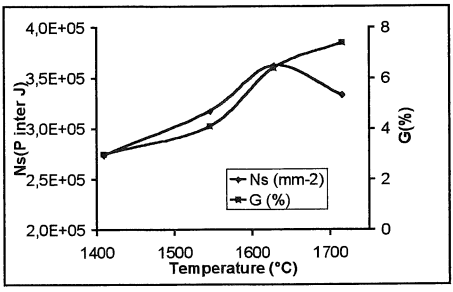

Figure 10 : Evolution of $N_S(P \cap J)$ and G as a function of temperature for a time of 60 mn.

Figure 9 shows that the swelling increases regularly with the time of processing. The number of bubbles per unit area of grain boundaries increases first, and then becomes constant.

Figure 10 shows the same evolution for the swelling as a function of the temperature. Moreover, N is going through a maximum. This means that the coalescence is more important than the creation of bubbles to high temperatures. These results have been used to construct a model for swelling by coalescence of bubbles from the initial hypotheses of Greenwood and. Speight (1963) and proposed by Zacharie (1997) and Zacharie et al (1998b).

ACKNOWLEDGEMENTS

This works was performed in the frame of the "Pôle Traitement et Analyse d'Images" Pôle TAI de Basse-Normandie, France.

REFERENCES

Beucher S, Meyer F. The morphological approach to segmentation: the watershed transformation. In Mathematical Morphology in Image Processing (Dougherty E Editor). Marcel Dekker, New York, 1992; pp 433-481.

Coster M, Chermant JL. Précis d'analyse d'images. Les Presses du CNRS. Paris 1989.

Greenwood GW, Speight MV. An analysis of the diffusion of fission gas bubbles and its effect on the behaviour of reactor fuels. J Nucl Mater 1963; 10: 140-150.

Grimaud M. La géodésie numérique en morphologie mathématique. Application à la détection automatique de microcalcifications en mammographie numérique. Thèse de Doctorat de l'Ecole des Mines de Paris, France 1991.

Serra J. Image Analysis and Mathematical Morphology. Academic Press London, 1982.

Zacharie I.Traitements thermiques de l'oxyde d'uranium irradié en réacteur à eau pressurisée. Gonflement et relachement des gaz de fission. Thèse de Doctorat de l'Ecole Centrale de Paris, France, 1997.

Zacharie I, Lansiart S, Combette P, Trotabas M, Coster M, Gross M. Thermal treatments of uranium oxide irradiated in pressurised water reactor: sweeling and realease of fission gases. To appear in J Nucl Mat 1998a.

Zacharie I, Lansiart S, Combette P, Trotabas M, Coster M, Gross M. Microstructural analysis and modelling of intergranular swelling of an irradiated UO_2 fuel treated at high temperature. To appear in J Nucl Mat 1998b.

Zeboudj R. Filtrage, seuillage automatique, contraste et contours: du prétraitement à l'analyse d'image. Thèse de Doctorat de l'Université de Saint Etienne, France, 1988.

Presented at the 7th European Congress for Stereology, Amsterdam, April 20th to 23rd, 1998.